

# Photonic Sintering of Silver Nanoparticles: Comparison of Experiment and Theory

Jeff West, Michael Carter, Steve Smith and James Sears  
*South Dakota School of Mines and Technology*  
USA

## 1. Introduction

Photonic sintering is a low thermal exposure sintering method developed to sinter nanoparticle thin films. The process involves using a xenon flash lamp to deliver a high intensity, short duration ( $< 1$  ms), pulse of light to the deposited nanoparticles. Photonic sintering was developed by Nanotechnologies (now NovaCentrix) of Austin, Texas, and was first made public in 2006 (Schroder et al., 2006). As photonic sintering is a new technology it is also known as pulsed thermal processing (PTP) (Camm et al., 2006) and intense pulsed light (IPL) sintering (Kim et al., 2009). Conductive thin films composed of nanoparticle depositions, when exposed to a short pulse of high intensity light, are transformed into functional printed circuits. The printed circuits can be tailored for use as flexible circuit boards, RFID tags, flat panel displays (Carter & Sears, 2007), photovoltaics, or smart packaging (Novacentrix, 2009). One of the primary advantages of the method is that the high intensity pulse of light produces minimal damage on low temperature substrates. This allows the nanoparticles to be deposited and cured on a high variety of low temperature substrates such as cloth, paper, and Mylar (Carter & Sears, 2007; Farnsworth, 2009). Another advantage of using photonic curing is the speed at which nanoparticle depositions can be sintered. Rather than spending hours in an oven or programming a laser to follow the deposition path, the photonic curing process can sinter large areas ( $\sim 200$  cm<sup>2</sup> per 10 cm long lamp) in  $< 2$  ms (Novacentrix 2009).

One of the main objectives of the work reported here was to determine the effectiveness of photonic sintering of silver nanoparticle depositions. This was done by measuring the densification of silver nanoparticle films following photonic sintering. The absorption of light emitted by a flash lamp for varying thicknesses of silver nanoparticle layers was also measured. To determine the amount and depth of sintering, SEM images were taken of a cross section of a sintered film. To better understand the process through which the nanoparticles are sintered, we calculate the absorption of the light emitted by the flash lamp by the silver nanoparticle film using the Bruggeman effective medium theory. Using the heat transfer software package Fluent™ to model the temperature profile of the films during and following sintering, we propose a model for the photonic process.

## 2. Photonic sintering overview

Photonic sintering was first introduced at the 2006 NSTI Nanotechnology Conference and Trade Show (Schroder et al., 2006). It was developed by NovaCentrix for the purpose of rapidly sintering metal nanoparticle based films (Schroder et al., 2006). The technology allows the nanoparticles to sinter without significantly raising the temperature of the substrate. This is accomplished by using a flash lamp. Two main parameters control the degree of sintering: the intensity of the lamp and the duration of the light pulse. The flash lamp is held between 0.5 cm to 20 cm above the deposition and an intense current is run through the flash lamp (Novacentrix, 2007). Due to this intense current, the xenon flash lamp issues a high intensity, broad spectrum pulse of light. This pulse of light is absorbed by the nanoparticles, which heats them to such a degree that they sinter into a single component.

Because photonic sintering has a minimal effect on the substrate, it enables nanoparticle films to be cured on low temperature substrates such as paper, Mylar, and PET. In addition to allowing low temperature substrates to be used, the speed at which the films are sintered allows the use of inks which would oxidize if sintered over long periods of time using traditional methods, such as copper (Novacentrix, 2009; Schroder 2006). Both of these advantages allow printed electronics manufacturers to reduce the cost of production by using lower cost substrates and less expensive inks.

The Novacentrix PCS-1100 Photonic Curing System is a research and development model in use at South Dakota School of Mines & Technology (SDSM&T). The PCS-1100 has a pulse duration that can be set from 35  $\mu\text{s}$  to 1000  $\mu\text{s}$  (Novacentrix, 2007). The voltage of the flash lamp (which controls the intensity and spectral distribution of the lamp) can also be adjusted with a maximum operational voltage of 4000V (Novacentrix, 2007). The PulseForge 3100 is a production model (currently in operation at Oak Ridge National Laboratory) that can be incorporated with a roll-to-roll production system or a conveyor belt to sinter continuous or discrete items (Novacentrix, 2009).

During the development of photonic sintering, three basic assumptions were considered for sintering nanoparticles: (i) nanoparticles are predominantly black, they should absorb light very well (Schroder, 2006), (ii) once light is absorbed by the nanoparticles, due to their high surface area to mass ratio, the nanoparticles would heat easily and sinter quickly, and (iii) as nanoparticle films are very thin, they would not retain heat very well and cool rapidly, minimizing damage to the substrate. Photonic sintering has been shown to sinter conductive nanoparticle metals (*e.g.*, silver, gold, and copper) as well as dielectric nanoparticles made of alumina, zirconia, barium titanate, and mica, as well as the soft magnetic materials cobalt, ferrite and iron-nickel permalloy (Carter & Sears, 2007).

A comparison of the resistivities obtained using furnace, laser, and photonic sintering was reported by Carter and Sears (Carter & Sears, 2007). For the comparison, two different silver inks were used. One ink was based on the AgSt2 Novacentrix 25 nm diameter silver nanoparticles and the other ink was composed of UT Dot 7 nm diameter silver nanoparticles. The inks were deposited into 1 cm<sup>2</sup> pads and sintered using various furnace temperatures, laser fluences, and flash lamp voltages. The resistivities were then measured and the lowest values obtained for each method. The lowest resistivities were found using

the following settings for each method. The furnace sintering was done at a temperature of 500°C for two hours. The laser sintering was done using a laser fluence of 2800 J/cm<sup>2</sup>. The photonic curing was done using a lamp voltage of 1200V with a pulse length of 900 μs. The lowest surface resistivity for each method is shown in Table 1. The measurements showed that the resistivity of the photonic sintered silver was comparable to the resistivity of the oven and laser sintered silver, and that smaller nanoparticles approach bulk silver resistivities after photonic or oven sintering.

<u>Material</u>	<u>Sintering Method</u>	<u>Resistivity (μΩ-cm)</u>
UT Dot (7 nm silver)	Furnace	2.1 ± 0.9
	Photonic	2.8 ± 0.8
AgSt2 (Novacentrix 25 nm silver)	Furnace	3.8 ± 0.3
	Laser	5.3 ± 0.3
	Photonic	7.9 ± 0.5
Bulk Silver		1.59

Table 1. Table comparing resistivities obtained using different sintering methods for two silver nanoparticle based inks.

### 3. Experimental results

After observing the comparisons to traditional sintering methods, experiments were run to gain insight into the process by which particles are sintered during photonic curing. The densification as a function of the flash lamp voltage and pulse duration was measured to determine the effects of those parameters. Depositions of varying thickness were tested using a UV-Vis spectrometer to measure the absorption of the depositions in the wavelength region produced by the flash lamp. Finally, SEM images were taken of the cross section of a thick sintered sample to determine the depth and amount of sintering in the deposition.

#### 3.1 Parametric study of densification

We measured the densification of silver nanoparticles as a function of the pulse duration and flash lamp voltage to find the optimal settings to sinter V2 silver ink. The V2 silver ink consists of Novacentrix 25 nm silver nanoparticles suspended in DMA. The measurements also allow a determination of the effect of lamp voltage and pulse duration on the sintering process.

The process of measuring the densification began by finding the volume fraction of nanoparticles in the deposition prior to sintering. This was accomplished by weighing a clean glass slide and then depositing V2 ink in a square pattern on the slide. The thickness of the deposition was then measured using a Zeiss Imager M1M microscope. The deposition thickness was determined by focusing on the surface of the glass slide and then again on the surface of the deposition. The focal distances were then compared to find the thickness of

the deposition. The glass slide with the deposition was then weighed again to find the total mass. The area and thickness of the deposition gave the total volume of the deposition and from the weight measurements the mass of the deposition was also known. The mass of the deposition was then divided by the density of silver to find the volume of the deposited silver. The calculated volume of the silver was then divided by the volume of the deposition to find the volume fraction of the silver in the deposition. The volume fraction of silver in the deposition was calculated to be 36% using this method with a density of the deposition being  $3.8 \text{ g/cm}^3$ .

After finding the volume fraction of the silver in the deposition prior to sintering, the next step was to deposit the material and measure the volume prior to and after sintering to determine the densification of the deposition. This was accomplished by depositing V2 silver ink in a 3 mm by 10 mm pad on a glass slide. The thickness of the deposition was measured using the Zeiss Imager M1M microscope. The deposition was then placed into the photonic curing system and sintered. The thickness of the deposition was then measured again. As the thickness was the only dimension to change during the sintering process the change in the volume was found. As the mass stayed approximately constant after sintering, the density of the deposition and volume fraction of silver in the deposition were then calculated. This process was completed ten times for each setting on the photonic curing system to obtain an adequate sampling size. The results are shown in Figure 1.

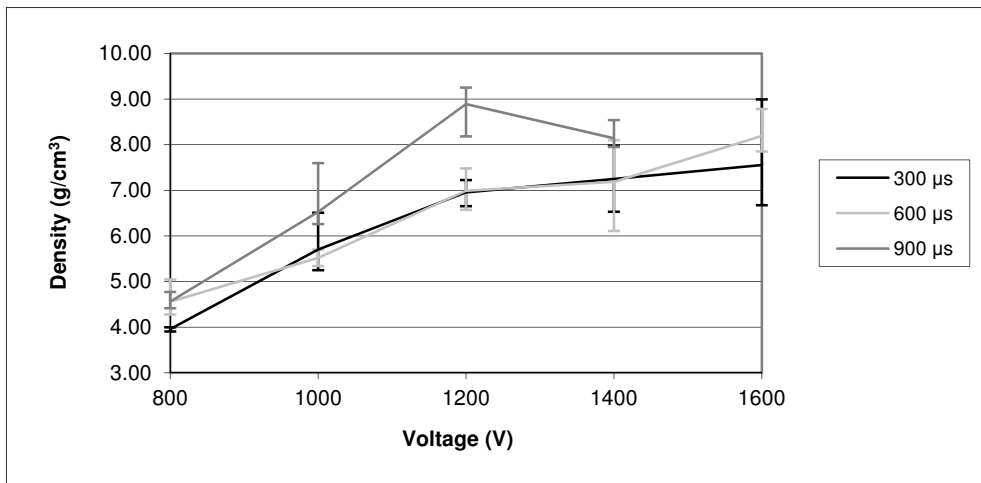


Fig. 1. Graph of Sintered Density vs. Flash Lamp Voltage.

Figure 1 shows that there is a definite optimum voltage setting for the photonic curing of the silver depositions tested. As the density of bulk silver is  $10.6 \text{ g/cm}^3$ , the average density using settings of  $900 \mu\text{s}$  and  $1200\text{V}$  of  $8.89 \text{ g/cm}^3$ , gives a volume fraction of 83.87% for the sintered silver. Figure 1 also shows that a longer pulse length produces a denser deposition than a shorter pulse. Using flash lamp voltages above  $1600\text{V}$  the depositions cracked and experienced blow off due to the high intensity of the light. This was taken as an upper limit to the voltages that can be used to sinter silver films using these pulse lengths.

### 3.2 Measurement of UV-vis spectrum absorption

To find which wavelengths and how much of the light output by the flash lamp are absorbed by different thicknesses of silver depositions, measurements of the absorption were made by a HP 8452A Diode Array Spectrophotometer. These measurements allowed us to determine the thickness of the silver deposition beyond which the light will no longer penetrate. To make these measurements, depositions were made on a quartz slide to minimize absorption and scattering effects from the substrate. The depositions were made using the GPD aerosol jet system to deposit V2 silver in 1 cm<sup>2</sup> pads. Thicknesses of 1.0, 3.1, and 5.0 μm were measured using the Zeiss Imager M1M microscope and taken to the HP 8452A Diode Array Spectrophotometer for the absorption measurements. The spectrophotometer takes a measurement of the absorption every 2 nm in wavelength, from 190 to 820 nm. The absorption is found by sending a pulse of light through the deposition and substrate to a sensor on the other side. The absorption is measured as the amount of light that does not reach the sensor. The spectrophotometer gives the results as the absorbance. The absorption is found using the equation

$$A = (1 - 10^{-a}) * 100, \quad (1)$$

where  $A$  is the absorption and  $a$  is the absorbance (Skoog, 1998). The results of the measurements are shown in Figure 2.

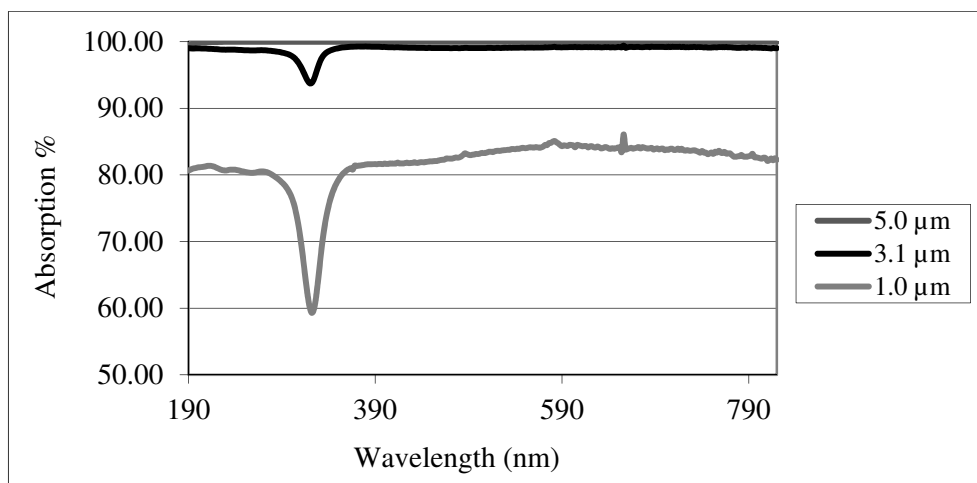


Fig. 2. Absorption vs. Wavelength for different thicknesses of V2 silver depositions.

Figure 2 shows that there is strong absorption of the light by the silver deposition at operational thicknesses. There is a drop in the absorption resulting in a minimum absorption at 322 nm. There is near total absorption of the light using the 3.1 μm thickness with the absorption after the minimum averaging 99%. There is complete absorption of the light for the 5.0 μm thickness. This indicates that if there is any sintering of silver beyond that thickness then it is due to thermal effects as there would be no light to impart energy to the deposition at that depth. The absorption measurements do not show the plasmon

resonance peak that has been observed in silver nanoparticles suspended in solution (Chen et al., 2004; Hutter et al., 2001; Lim et al., 2005). This indicates that the absorption for silver nanoparticle films with volume fractions of 30% or higher of silver, more closely mimic the absorption properties of bulk silver than of nanoparticle silver. Figure 2 also shows that the V2 silver absorbs the light strongly in the visible portion of the spectrum which is the area where bulk silver reflects a majority of the light. These measurements show that for the UV and visible spectrums of light the V2 silver consistently absorbs a majority of the light output from the lamp allowing photonic sintering to take place.

### 3.3 SEM Imaging of microstructure

SEM images were taken of a cross section of photonicallly cured V2 silver to determine the depth and amount of sintering in a deposition beyond the thickness light will penetrate. Twenty six layers of V2 silver were deposited in a 1 cm<sup>2</sup> area upon a glass slide using the GPD aerosol jet system. The deposition was then cured using a 900  $\mu$ s, 1200 V pulse of light from the photonic curing system. After etching, the slide was broken in half to provide a cross section of the deposition. One of the slide halves was embedded in an epoxy mold for mounting and polishing followed by examination in the SEM. An image was taken using the Zeiss optical microscope to show the thickness of the deposition in cross section. This image is shown in Figure 3. The thickness of the silver cross section after sintering was measured to be 21.59  $\mu$ m.



Fig. 3. Optical cross section of the V2 silver on a glass slide in an epoxy mold.

The SEM images that were taken show that slightly over half of the deposition was sintered, while there are substantial voids in the section of deposition closest to the glass. A SEM image of the silver deposition cross section is shown in Figure 4. Figure 4 shows approximately 11  $\mu$ m of sintered silver which proves that there is a heat transfer effect in photonic curing. This is shown by densification beyond the penetration of the light as the

light does not penetrate more than 5  $\mu\text{m}$  into the deposition. The voids in the deposition are a consequence of the polishing procedure and show that that portion of the deposition was not sintered. Figure 4 shows a silver volume fraction of approximately 80%. This is consistent with the densification measurements made in Figure 1.

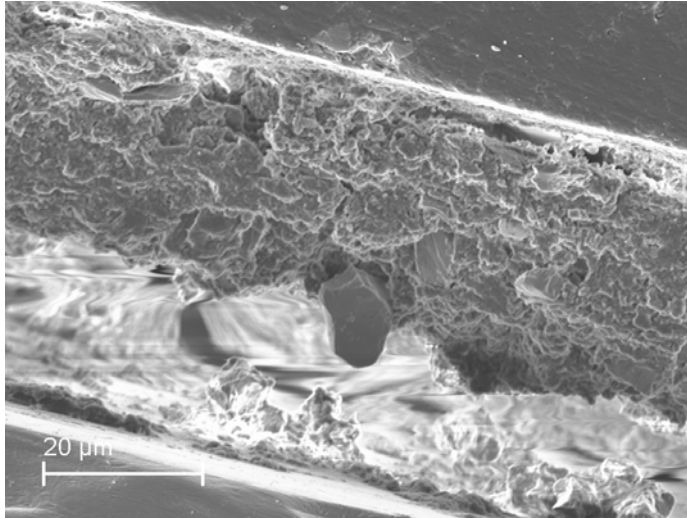


Fig. 4. SEM image of silver deposition cross section.

As thickness measurements were not made prior to sintering the silver, due to problems with the Zeiss microscope software, the actual volume reduction was not found. However, the previous densification measurements can be used to assist in back calculating the thickness of the deposition prior to sintering. Using the observed silver volume fraction of 80% throughout the 11  $\mu\text{m}$  sintered thickness, the 11  $\mu\text{m}$  thickness that was sintered is calculated to have been 24.6  $\mu\text{m}$  thick prior to sintering. 24.6  $\mu\text{m}$  is much thicker than the 5  $\mu\text{m}$  depth at which the light can no longer penetrate. The calculated thickness of the sintered area prior to sintering was combined with the approximately 10.6  $\mu\text{m}$  thickness that was not sintered, which gives the total thickness of the deposition of 35.2  $\mu\text{m}$ .

#### 4. Optical absorption in metallic nanoparticle composites

Effective medium theories have been used to calculate the effective dielectric constant for particles within a medium. The effective medium theories that appear the most often in the literature are the Maxwell-Garnett and Bruggeman effective medium theories. The Maxwell-Garnett effective medium theory was originated in 1904 by J.C. Maxwell Garnett (Maxwell Garnett, 1904). The Maxwell-Garnett theory is only applicable when encountering low volume fractions of material, typically below the percolation threshold or a volume fraction below 30% (Claro & Rojas, 1991; Datta et al., 1993; Davis & Schwartz, 1985; Gibson & Buhrman, 1983; Grechko et al., 2000; Lamb et al., 1980; Li et al., 2006; Lidorikis et al., 2007;

Stroud & Pan, 1978; Wang et al., 2005; Yannopoulos, 2006). However, other papers have demonstrated that the Maxwell-Garnett effective medium theory will work for higher volume fractions (Fu et al., 1993; Mallet et al., 2005). The Maxwell-Garnett dielectric function is defined by the expression:

$$\frac{\varepsilon - \varepsilon_b}{\varepsilon + 2\varepsilon_b} = f_a \frac{\varepsilon_a - \varepsilon_b}{\varepsilon_a + 2\varepsilon_b}, \quad (2)$$

where  $\varepsilon$  is the dielectric function of the effective medium,  $\varepsilon_a$  is the dielectric function of the particles in the medium,  $\varepsilon_b$  is the dielectric function of the medium, and  $f_a$  is the volume fraction of the particles contained in the medium (Aspnes, 1982).

The Bruggeman effective medium approximation was formulated in 1935 by D.A.G. Bruggeman (Bruggeman, 1935). Unlike the Maxwell-Garnett model the Bruggeman model does not have a preference toward the embedded particle or the medium, the Bruggeman model treats the inclusions and medium equally (Aspnes, 1982; Landauer, 1978). The Bruggeman model has been used to calculate the dielectric constant of particles embedded in materials and compared with the measured values (Brosseau, 2002; Chen, L.Y. & Lynch, 1987; Mendoza-Galván et al., 1994; Rousselle et al., 1993). The Bruggeman model has also been modified to better model the dielectric constant of nonlinear media and different shaped particles (Goncharenko, 2003; Pellegrini 2001). The Bruggeman dielectric function has been shown to work well with higher volume fractions (Bohren & Huffman, 1983; Bruggeman, 1935). The Bruggeman dielectric function is defined by the expression:

$$f_a \frac{\varepsilon_a - \varepsilon}{\varepsilon_a + 2\varepsilon} + f_b \frac{\varepsilon_b - \varepsilon}{\varepsilon_b + 2\varepsilon} = 0, \quad (3)$$

where  $\varepsilon$  is the dielectric function of the effective medium,  $\varepsilon_a$  is the dielectric function of the particles in the medium,  $\varepsilon_b$  is the dielectric function of the medium,  $f_a$  is the volume fraction of the particles contained in the medium, and  $f_b$  is the volume fraction of the particles contained in the medium (Aspnes, 1982). Once the average dielectric function is found, the imaginary portion of the refractive index and the absorption coefficient for the effective medium can be calculated by the expression:

$$\alpha' = \frac{4\pi k}{\lambda}, \quad (4)$$

where  $k$  is the imaginary part of the refractive index and  $\lambda$  is the wavelength of light (Skoog et al., 1998). From this, using the Beer-Lambert law (Skoog et al., 1998), the absorption spectra can be calculated.

To test the models, the absorption coefficients for 30% silver in air was calculated using the Maxwell-Garnett and Bruggeman models and compared with the absorption coefficient for bulk silver. The comparison is shown in Figure 5. From Figure 5 it is observed that the absorption coefficients obtained using the effective medium models are lower than for bulk silver. In the UV range of the spectrum the effective medium models match well and have the same dip at the 318 nm wavelength. The absorption coefficient minimum at 318 nm corresponds to the absorption minimum observed in the UV-Vis measured absorption. This indicates the measured absorption dip is a property of bulk silver and not an effect of the plasmon resonance. After the absorption coefficient dip the data from the models begins to

diverge. The absorption coefficient from the Maxwell-Garnett model rises sharply, becomes higher than for bulk silver, and peaks at the 380 nm wavelength mark. This peak in the absorption coefficient is near the surface plasmon resonance that has been seen in the literature for silver nanoparticles dispersed in an aqueous solution (Chen, T.C. et al., 2004; Hutter et al., 2001; Lim et al., 2005). The Maxwell-Garnett data then drops rapidly to near zero for the remainder of the modeled wavelength area. After the 318 nm wavelength mark the Bruggeman data gently rises for the remainder of the wavelengths modeled. Thus the Bruggeman model will most closely matches the measured data in our experiments.

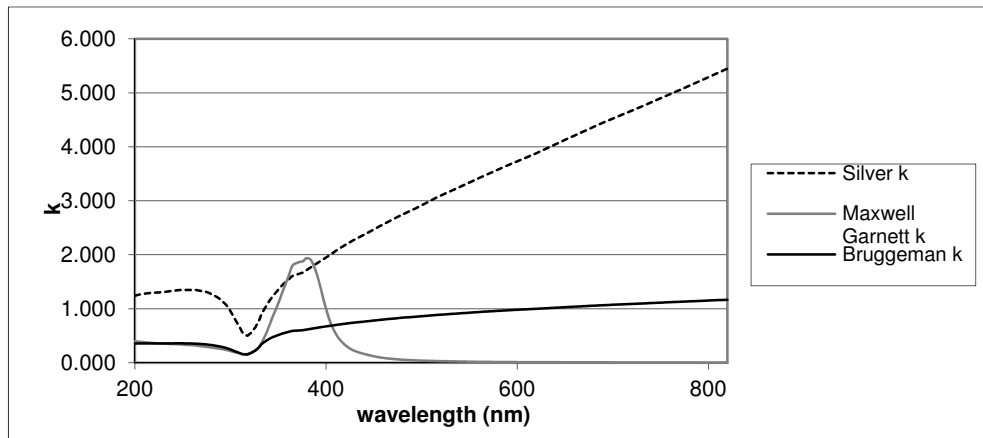


Fig. 5. Comparison of the absorption coefficients for 30% silver in air using Maxwell-Garnett and Bruggeman effective medium models with the values for bulk silver.

To obtain a closer look at how the Bruggeman absorption curve and the measured absorption curve compare, the thickness of the deposition for the Bruggeman model was set to 160 nm and is shown in Figure 6 compared with the 1.3  $\mu\text{m}$  thick measured absorption. The absorption minimums in Figure 6 are 62% for the Bruggeman model at 316 nm and 64% at 322 nm for the measured silver. In the UV and near IR regimes the absorption curves have a similar slope. After the absorption minimum the Bruggeman model absorption is relatively constant through the visible spectrum while the measured data rises constantly before leveling off. Though the absorption as modeled using the Bruggeman effective medium theory is stronger than what was measured, unlike the Maxwell-Garnett model, the Bruggeman model closely follows the measured absorption dip and does not decrease significantly at longer wavelengths. The discrepancy in the theoretical and experimental thicknesses would suggest that most of the absorption takes place near the surface of the film. However, the spectral characteristics of the Bruggeman model reproduce very well the experimental data, and thus were used to model the absorption of the deposited materials in this work.

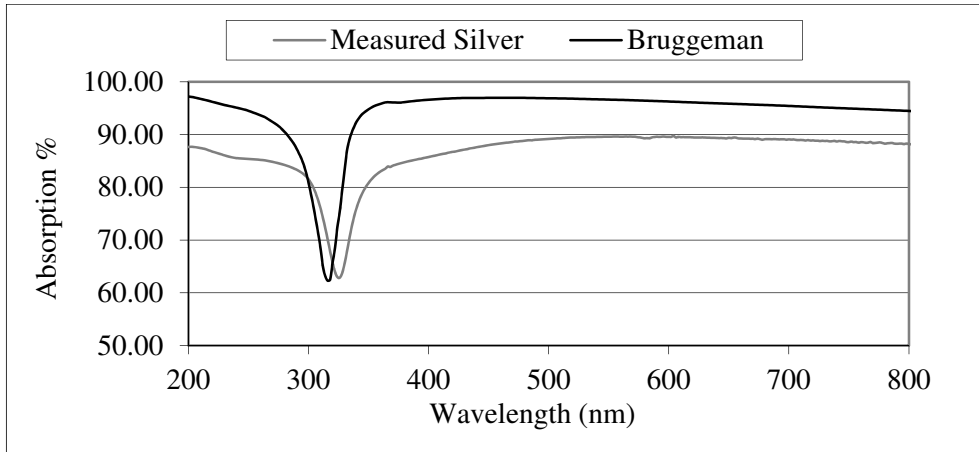


Fig. 6. Absorption vs. wavelength for 30% volume fraction silver, 160 nm thick film using Bruggeman model and a 1.3  $\mu\text{m}$  thick measured silver film.

#### 4.1 Modifying the bruggeman model with the extended drude model

As the calculated absorption using the Bruggeman model does not perfectly match the measured absorption, the complex dielectric function was modified using the extended Drude model in an attempt to bring the calculated and measured absorption closer together (Haiss et al., 2007; Kreibig & Vonfrags, 1969). The extended Drude model was used to modify the dielectric function of silver for particle diameters of 25 nm and 5 nm. The absorption was then calculated using a volume fraction of 30% and a film thickness of 150 nm and compared with the measured absorption and the unmodified Bruggeman model. This is shown in Figure 7. The thickness of the film was thinned to 150 nm to bring the modified Bruggeman model with the 25 nm diameter silver particles in line with the measured silver absorption. Figure 7 shows that in the UV portion of the spectrum the particle size did not affect the absorption of the silver film. The particle size did affect the absorption minimum slightly with the minimum occurring at 314 nm for the 5 nm diameter silver with a minimum absorption of 68.5%. The 5 nm diameter silver also had a calculated absorption in the visible range slightly below the unmodified Bruggeman and Drude modified Bruggeman absorptions. The 25 nm diameter calculated absorption using the extended Drude and Bruggeman models agreed well with the unmodified Bruggeman calculated absorption in the UV and visible ranges. The main difference was that the absorption minimum at 316 nm was 3.5% stronger for the Drude modified Bruggeman model than for the unmodified Bruggeman absorption. These comparisons indicate that the particle size does not play a large role in the absorption by nanoparticle films with volume fractions of 30% or greater. The nanoparticle silver films appear to act more like bulk silver than like individual silver nanoparticles. This is shown through a surface plasmon resonance peak not appearing in the measured absorptions. The reason for the absorption appearing to be so strong in the calculated absorptions as opposed to the measured data could be due to the majority of the absorption occurring within the first few hundred nanometers of the films, with the absorption only slightly increasing beyond that depth.

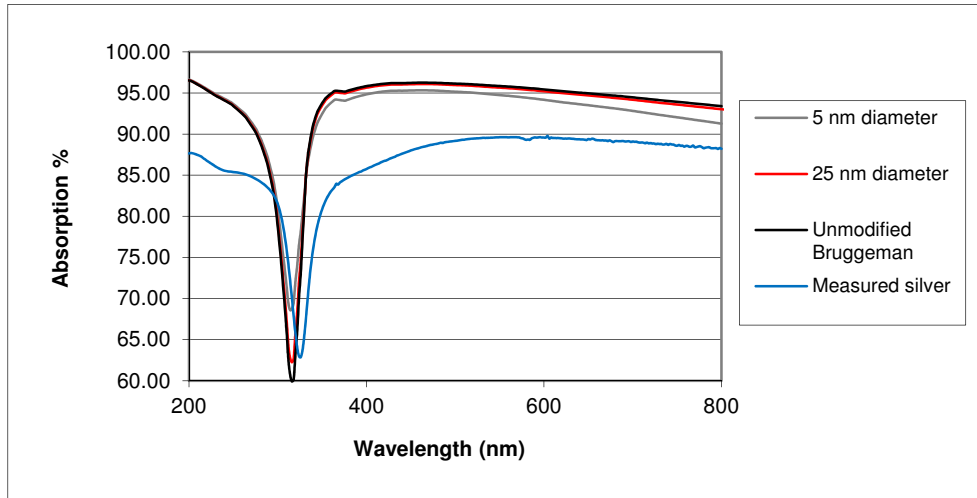


Fig. 7. Absorption vs. Wavelength for a 30% volume fraction of silver, 150 nm thick film calculated using the unmodified Bruggeman model, the Bruggeman model modified by the extended Drude model for particle diameters of 5 nm and 25 nm, and for a 1.3  $\mu\text{m}$  thick measured silver film.

## 5. Modeling of sintering processes using fluent

The Gambit modeling software and Fluent heat transfer software were used to create a slab of material and model the heat transfer through the slab. Fluent and Gambit are two software programs that model fluid flow and heat transfer through solids and fluids. In Gambit the volume and boundaries are created and then the created volume is transferred to Fluent. In Fluent the material and boundary conditions are input, the energy equation and other thermal models are activated, and the simulation is run. Using the Gambit and Fluent software, a 10  $\mu\text{m}$  thick, 100  $\times$  100  $\mu\text{m}$  wide and long slab of silver was created that would absorb radiative energy along its top surface and was surrounded by air and had a substrate of glass. In Fluent the temperature of the silver and the amount of silver melted as a result of the energy absorption were simulated.

The Fluent simulation used boundary conditions of convective cooling for the sides and top of the silver slab, conductive cooling through the glass substrate, and radiative heating on the top surface of the slab. The volume fraction of silver in the slab was set to 0.33 with the remainder of the volume taken up with air. The melting point of the silver was set to the observed value of 600°C. The ambient temperature surrounding the slab was set to 21°C and the glass substrate thickness was set to 18  $\mu\text{m}$  for computational efficiency. The simulated silver slab was heated using a flash lamp voltage of 1200V and a pulse duration of 900  $\mu\text{s}$ . The heat transfer coefficient between the silver and the air was set to 3500  $\text{W}/\text{m}^2\text{K}$ . Following heating, the slab was allowed to cool for 900  $\mu\text{s}$ . The temperature and the amount of melting was measured every 100  $\mu\text{s}$ . The temperature profile of the silver slab from the simulation is shown in Figure 8.

From Figure 8 it is shown that the simulated temperature reaches the melting point of the nanosilver by 200  $\mu\text{s}$ . After spending 500  $\mu\text{s}$  at 600°C the temperature of the slab begins to rise again. Once the flash lamp pulse is turned off the silver slab cools rapidly. The silver slab solidifies within 100  $\mu\text{s}$  and cools to a temperature below 100°C within 800  $\mu\text{s}$  of the pulse ceasing which matches observations of the slab being room temperature upon immediate removal from the photonic sintering system.

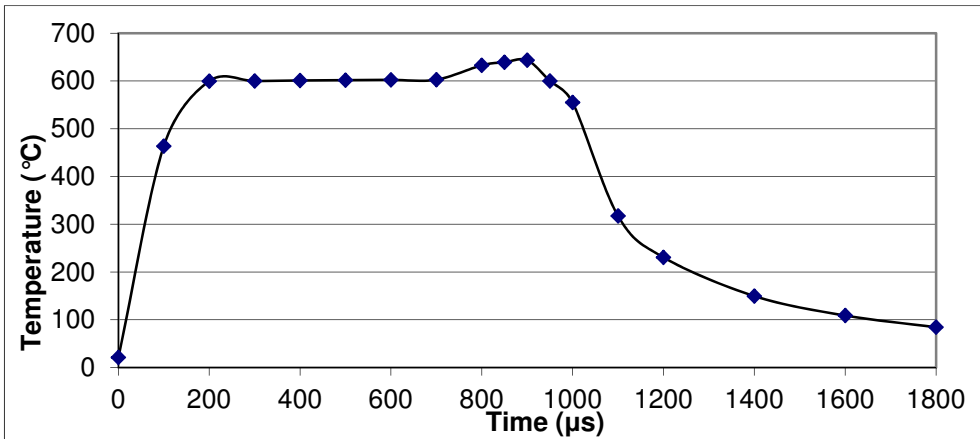


Fig. 8. Temperature vs. Time for a 10  $\mu\text{m}$  thick silver slab on a glass substrate with a flash lamp voltage of 1200V for 900  $\mu\text{s}$ .

To complement the temperature profile, the liquid fraction at the top, center, and bottom of the slab was also modeled. The liquid fraction of the slab is shown in Figure 9. The silver has slightly melted at 200  $\mu\text{s}$  and by 700  $\mu\text{s}$  the top surface of the silver has completely melted.

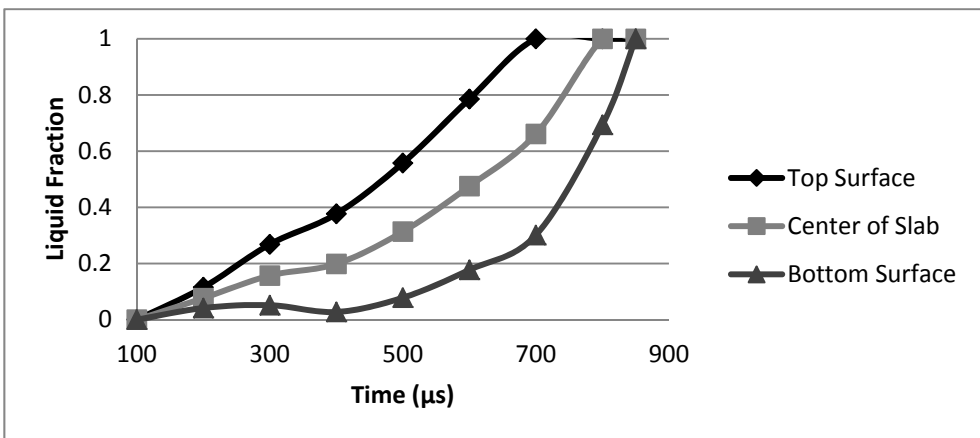


Fig. 9. Liquid Fraction vs. Time for three positions on the silver slab.

The bottom surface of the silver takes until 850  $\mu\text{s}$  to completely melt. After the top surface of the silver has completely melted the temperature begins to rise again as seen in Figure 8. This matches the premise based on the densification measurements and simulation data that at 300  $\mu\text{s}$  the silver has just begun to melt, the melting is still in progress at 600  $\mu\text{s}$ , and the material has completely melted by 900  $\mu\text{s}$ . This gives a relatively slow melting time allowing the material to sinter at a rate that will not crack or ablate the material off the substrate.

After simulating the temperature of the 10  $\mu\text{m}$  thick silver slab on glass the silver slab was thinned to 3  $\mu\text{m}$ , as 3  $\mu\text{m}$  is the typical deposition thickness. For the thinner slab some conditions were modified to make them more accurate. The porosity of the silver slab remained at 33%. The heat transfer coefficient was set to 3100  $\text{W}/\text{m}^2\text{K}$  as the simulations on glass showed the silver remaining near 600°C. The emissivity was set to 0.99 to allow the appropriate amount of the pulse to pass through the deposition. The melting temperature remained at 600°C and the ambient temperature was set to 21°C. The flash lamp voltage was set to 1200V and the pulse was set to a length of 900  $\mu\text{s}$ , after which 900  $\mu\text{s}$  of cooling was simulated. The thickness of the glass substrate was increased to 20  $\mu\text{m}$ . The resultant graph of temperature versus time is shown in Figure 10. From observing the liquid fraction the simulation indicates that for the thinner slab the deposition has melted 93% after the pulse has been active for 100  $\mu\text{s}$ . The temperature reaches 701°C by 200  $\mu\text{s}$  and then decreases to 644°C at 300  $\mu\text{s}$  and proceeds to increase at a constant rate for the duration of the pulse. Once the pulse ends the temperature rapidly decreases. One difference from using the 3  $\mu\text{m}$  slab instead of the 10  $\mu\text{m}$  slab is the early peak of slab temperature at 200  $\mu\text{s}$ . Another difference is that the thinner slab melts quicker, which is expected as the thin slab is absorbing nearly the same amount of energy and has less mass to heat.

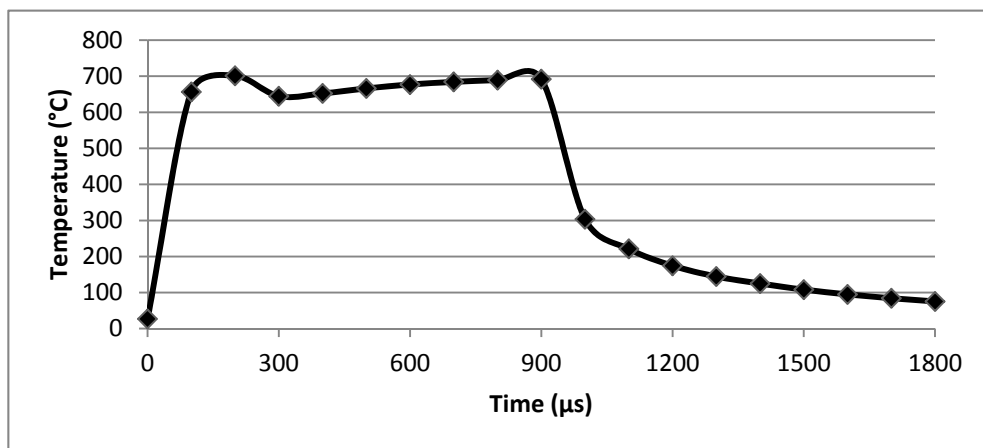


Fig. 10. Temperature vs. time for a 3  $\mu\text{m}$  thick silver slab using a 1200V flash lamp voltage and a 900  $\mu\text{s}$  pulse length using Fluent.

## 6. Conclusions

In examining the photonic sintering process a number of interesting results were found. It was shown that there is significant densification of the photonic sintered silver, with

the photonic sintered silver reaching 84% of the density of bulk silver. It was observed that there is an optimum flash lamp voltage, beyond which the silver nanoparticle film becomes damaged through cracking and blow off. UV-Vis spectroscopy shows that the silver nanoparticle films absorb in excess of 80% of the light emitted by the flash lamp at operational thicknesses, with total absorption occurring at a thickness of 5  $\mu\text{m}$ . The UV-Vis spectroscopy also showed that the light absorption by the uncured silver films is broadband, and that the plasmon resonance is not the dominating feature of the absorption. This indicates the absorption of the silver films acts like that of bulk silver rather than that of individual silver nanoparticles. Sintering a 35  $\mu\text{m}$  thick silver deposition with the optimal pulse of 1200 V and pulse length of 900  $\mu\text{s}$ , the deposition decreased in thickness to 21.6  $\mu\text{m}$ . Of the sintered thickness of 21.6  $\mu\text{m}$ , 11  $\mu\text{m}$  was sintered to a volume fraction of 80% dense, while 10.6  $\mu\text{m}$  of the sintered thickness did not sinter. This proves that photonic sintering involves heat transfer between nanoparticles and that the photonic sintering process does not solely depend on the amount of light absorbed by each nanoparticle.

After deriving the equations and calculating the light absorption by silver nanoparticle films based on the Maxwell-Garnett effective medium theory and the Bruggeman effective medium approximation, the Bruggeman model matched the measured absorption the best. This result shows that to obtain the best match with the measured data, the nanoparticles should be considered as an effective medium, and that the effective medium theory used should be valid above the percolation threshold. Modifying the Bruggeman model with the extended Drude model showed that the absorption does not have a strong dependence on the particle size. The absorption models indicate that the majority of the absorption takes place within a few hundred nanometers of the surface of the film.

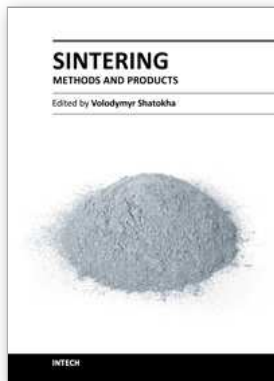
The temperature simulations using the heat transfer software Fluent indicate that the nanoparticle films melt within 300  $\mu\text{s}$  from the beginning of the pulse during the photonic sintering process. This result indicates that traditional solid state sintering models do not apply to photonic sintering. The Fluent simulations also showed that the temperature throughout the deposition does not vary to a wide extent. However, the liquid fraction of silver at various locations within the film can vary greatly depending on the speed of the melting process and the thickness of the silver layer.

## 7. References

- Aspnes, D.E. (1982). Local-field effects and effective-medium theory: A microscopic perspective. *Am. J. Phys.* Vol. 50, No. 8, pp. 704-709.
- Bohren, C. F. and Huffman, D. R. (1983). *Absorption and Scattering of Light by Small Particles*. New York: John Wiley & Sons, Inc.
- Brosseau, C. (2002). Generalized effective medium theory and dielectric relaxation in particle-filled polymeric resins. *Journal of Applied Physics*. Vol. 91, No. 5, pp. 3197-3204.
- Bruggeman, D.A.G. (1935). Berechnung verschiedener physikalischer Konstanten von heterogenen Substanzen. *Annalen der Physik (Leipzig)*. Vol. 24, pp. 636-679.
- Camm, D.M., Gelpy, J.C., Thrum, T., Stuart, G.C., and McCoy, S. (2006). Flash-Assist RTP for Ultra-Shallow Junctions. *JOM*, Vol. 58, No. 6, pp. 32-34.

- Carter, M. and Sears, J. (2007). Photonic Curing for Sintering of Nano-Particulate Material. *Advances in Powder Metallurgy & Particulate Materials – 2007: Proceedings of the 2007 International Conference on Powder Metallurgy & Particulate Materials, May 13-16, Denver, Colorado.*
- Chen, L.Y., Lynch, D.W. (1987). Effect of liquids on the Drude dielectric function of Ag and Au films. *Physical Review B*. Vol. 36, No. 3, pp. 1425-1431.
- Chen, T.C., Su, W.K., and Lin, Y.L. (2004). A Surface Plasmon Resonance Study of Ag Nanoparticles in an Aqueous Solution. *Japanese Journal of Applied Physics*, Vol. 43, pp. L119-L122.
- Chen, T.C., Su, W.K., and Lin, Y.L. (2004). A Surface Plasmon Resonance Study of Ag Nanoparticles in an Aqueous Solution. *Japanese Journal of Applied Physics*. Vol. 43, pp. L119-L122.
- Claro, F., Rojas, R. (1991). Correlation and multipolar effects in the dielectric response of particulate matter: An iterative mean-field theory. *Physical Review B*. Vol. 42, No. 8, pp. 6369-6375.
- Datta, S., Chan, C.T., Ho, K.M., Soukoulis, C.M. (1993). Effective dielectric constant of periodic composite structures. *Physical Review B*. Vol. 48, No. 20, pp. 14936-14943.
- Davis, V.A., Schwartz, L. (1985). Electromagnetic propagation in close-packed disordered suspensions. *Physical Review B*. Vol. 31, No. 8, pp. 5155-5165.
- Farnsworth, Stan. Curing Copper and other Thin-Film Materials at Production Speeds. *SEMICON West*. Moscone Center, San Francisco. 16 July 2009.
- Fu, L., Macedo, P.B., Resca, L. (1993). Analytic approach to the interfacial polarization of heterogeneous systems. *Physical Review B*. Vol. 47, No. 20, pp. 13818-13829.
- Gibson, U.J. and Buhrman, R.A. (1983). Optical response of Cermet composite films in the microstructural transition region. *Physical Review B*. Vol. 27, No. 8, pp. 5046-5051.
- Goncharenko, A.V. (2003). Generalizations of the Bruggeman equation and a concept of shape-distributed particle composites. *Physical Review E*. Vol. 68, 041108.
- Grechko, L.G., Whites, K.W., Pustovit, V.N., Lysenko, V.S. (2000). Macroscopic dielectric response of the metallic particles embedded in host dielectric medium. *Microelectronics Reliability*. Vol. 40, pp. 893-895.
- Haiss, W., Thanh, N., Aveyard, J., and Fernig, D. (2007). Determination of Size and Concentration of Gold Nanoparticles from UV-Vis Spectra. *Analytical Chemistry*. Vol. 79, pp. 4215-4221.
- Hutter, E., Fendler, J.H., and Roy, D. (2001). Surface Plasmon Resonance Studies of Gold and Silver Nanoparticles Linked to Gold and Silver Substrates by 2-Aminoethanethiol and 1,6-Hexanedithiol. *J. Phys. Chem. B*, Vol. 105, pp. 11159-11168.
- Hutter, E., Fendler, J.H., and Roy, D. (2001). Surface Plasmon Resonance Studies of Gold and Silver Nanoparticles Linked to Gold and Silver Substrates by 2-Aminoethanethiol and 1,6-Hexanedithiol. *J. Phys. Chem. B*. Vol 105, pp. 11159-11168.
- Kim, H.S., Dhage, S.R., Shim, D.E., and Hahn, H.T. (2009). Intense pulse light sintering of copper nanoink for printed electronics. *Applied Physics A*, Vol. 97, pp. 791-798.
- Kreibig, U. and Vonfrags. C. (1969). The Limitation of Electron Mean Free Path in Small Silver Particles. *Z. Physik*. Vol. 224, pp. 307-323.
- Lamb, W., Wood, D.M., Ashcroft, N.W. (1980). Long-wavelength electromagnetic propagation in heterogeneous media. *Physical Review B*. Vol. 21, No. 6, pp. 2248-2266.

- Landauer, R. (1978). Electrical conductivity in inhomogeneous media. *AIP Conference Proceedings*. Vol. 40, No. 1, pp. 2-45.
- Li, J., Sun, G., Chan, C.T. (2006). Optical properties of photonic crystals composed of metal-coated spheres. *Physical Review B*. Vol. 73, 075117.
- Lidorikis, E., Egusa, S., Joannopoulos, J.D. (2007). Effective medium properties and photonic crystal superstructures of metallic nanoparticle arrays. *Journal of Applied Physics*. Vol. 101, 054304.
- Lim, S.K., Chung, K.J., Kim, C.K., Shin, D.W., Kim, Y.H., and Yoon, C.S. (2005). Surface-plasmon resonance of Ag nanoparticles in polyimide. *Journal of Applied Physics*, Vol. 98, No. 8, 084309.
- Lim, S.K., Chung, K.J., Kim, C.K., Shin, D.W., Kim, Y.H., and Yoon, C.S. (2005). Surface-plasmon resonance of Ag nanoparticles in polyimide. *Journal of Applied Physics*. Vol. 98, No. 8, 084309.
- Mallet, P., Guérin, C.A., Sentenac, A. (2005). Maxwell-Garnett mixing rule in the presence of multiple scattering: Derivation and accuracy. *Physical Review B*. Vol. 72, 014205.
- Maxwell Garnett, J. C. (1904). Colors in metal glasses and in metallic films. *Philos. Trans. R. Soc.*, Vol. A203, pp. 385-420.
- Mendoza-Galván, A., Martínez, G., Martínez, J.L. (1994). Effective dielectric function modeling of inhomogeneous and anisotropic silver films. *Physica A*. Vol. 207, pp. 365-371.
- Novacentrix. (2007). *PCS-1100 Photonic Curing System Operations and Safety Manual*. Austin: Novacentrix Corp.
- Novacentrix. (2009). *PulseForge 3100 Development and Production: Metals Processing*. Available from <<http://www.novacentrix.com/product/pf3100.php>>.
- Novacentrix. (2009). *PulseForge 3300 Development and Production: Semiconductor and Photovoltaic Materials Processing*. Available from <<http://www.novacentrix.com/product/pf3300.php>>.
- Pellegrini, Y.P. (2001). Self-consistent effective-medium approximation for strongly nonlinear media. *Physical Review B*. Vol. 64, 134211.
- Rousselle, D., Berthault, A., Acher, O., Bouchaud, J.P., Zérah, P.G. (1993). Effective medium at finite frequency: Theory and experiment. *Journal of Applied Physics*. Vol. 74, No. 1, pp. 475-479.
- Schroder, K.A., McCool, S.C., and Furlan, W.R. (2006). Broadcast Photonic Curing of Metallic Nanoparticle Films. *Technical Proceedings of the 2006 NSTI Nanotechnology Conference and Trade Show, Volume 3*, pp. 198-201.
- Skoog, D., Holler, F. J., Nieman, T. (1998). *Principles of Instrumental Analysis*. Thompson Learning.
- Stroud, D., Pan, F.P. (1978). Self-consistent approach to electromagnetic wave propagation in composite media: Application to model granular metals. *Physical Review B*. Vol. 17, No. 4, pp. 1602-1610.
- Wang, J., Lau, W.M., Li, Q. (2005). Effects of particle size and spacing on the optical properties of gold nanocrystals in alumina. *Journal of Applied Physics*. Vol. 97, 114303.
- Yannopoulos, V. (2006). Effective-medium description of disordered photonic alloys. *J. Opt. Soc. Am. B*. Vol. 23, No. 7, pp. 1414-1419.



## **Sintering - Methods and Products**

Edited by Dr. Volodymyr Shatokha

ISBN 978-953-51-0371-4

Hard cover, 316 pages

**Publisher** InTech

**Published online** 23, March, 2012

**Published in print edition** March, 2012

This book is addressed to a large and multidisciplinary audience of researchers and students dealing with or interested in sintering. Though commonly known as a method for production of objects from fines or powders, sintering is a very complex physicochemical phenomenon. It is complex because it involves a number of phenomena exhibiting themselves in various heterogeneous material systems, in a wide temperature range, and in different physical states. It is multidisciplinary research area because understanding of sintering requires a broad knowledge - from solid state physics and fluid dynamics to thermodynamics and kinetics of chemical reactions. Finally, sintering is not only a phenomenon. As a material processing method, sintering embraces the wide group of technologies used to obtain such different products as for example iron ore agglomerate and luminescent powders. As a matter of fact, this publication is a rare opportunity to connect the researchers involved in different domains of sintering in a single book.

### **How to reference**

In order to correctly reference this scholarly work, feel free to copy and paste the following:

Jeff West, Michael Carter, Steve Smith and James Sears (2012). Photonic Sintering of Silver Nanoparticles: Comparison of Experiment and Theory, Sintering - Methods and Products, Dr. Volodymyr Shatokha (Ed.), ISBN: 978-953-51-0371-4, InTech, Available from: <http://www.intechopen.com/books/sintering-methods-and-products/photonic-sintering-of-silver-nanoparticles-comparison-of-experiment-and-theory>

**INTECH**  
open science | open minds

### **InTech Europe**

University Campus STeP Ri  
Slavka Krautzeka 83/A  
51000 Rijeka, Croatia  
Phone: +385 (51) 770 447  
Fax: +385 (51) 686 166  
[www.intechopen.com](http://www.intechopen.com)

### **InTech China**

Unit 405, Office Block, Hotel Equatorial Shanghai  
No.65, Yan An Road (West), Shanghai, 200040, China  
中国上海市延安西路65号上海国际贵都大饭店办公楼405单元  
Phone: +86-21-62489820  
Fax: +86-21-62489821

© 2012 The Author(s). Licensee IntechOpen. This is an open access article distributed under the terms of the [Creative Commons Attribution 3.0 License](#), which permits unrestricted use, distribution, and reproduction in any medium, provided the original work is properly cited.